AD-A062 799 BRISTOL UNIV (ENGLAND) H H WILLS PHYSICS LAB F/G 11/4
THE PHYSICAL MECHANISMS RESPONSIBLE FOR THE WEATHERING OF EPOXY--ETC(U)
OCT 78 T W TURNER, K H ASHBEE DA-ERO-76-G-068

UNCLASSIFIED NL

| OF |
AD A062799

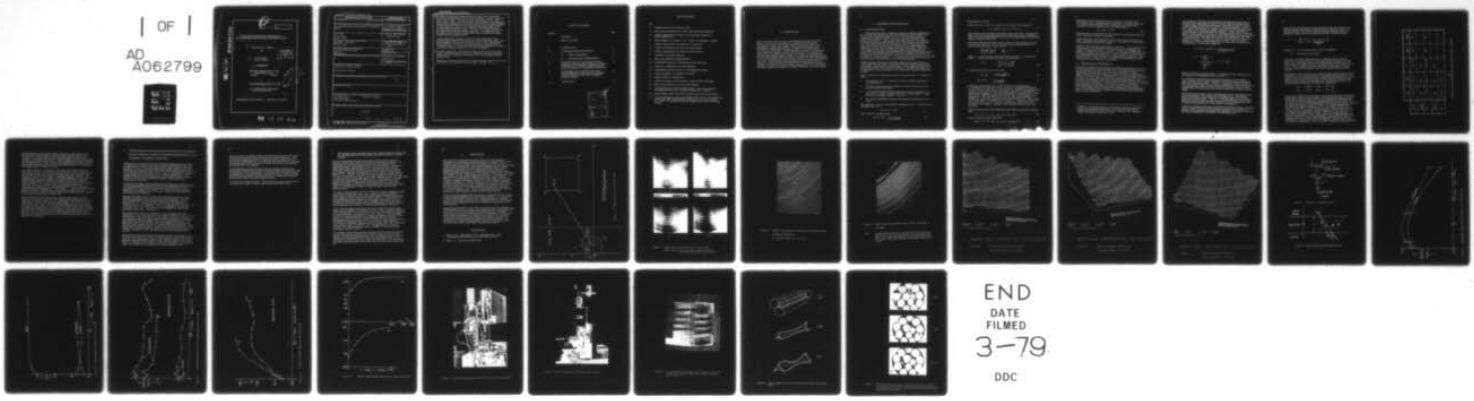

END
DATE FILMED
3-79
DDC

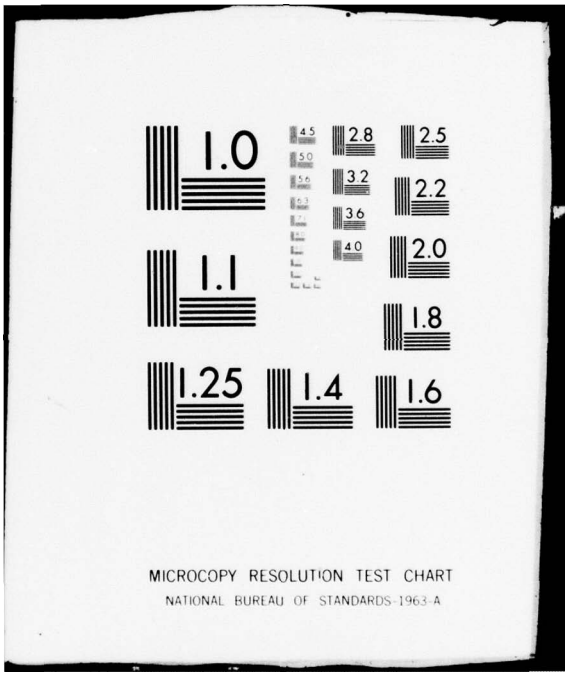
1.0
1.1
1.25
1.4
1.6
1.8
2.0
2.2
2.5
2.8
3.2
3.6
4.0
4.5
5.0
5.6
6.3
MICROCOPY RESOLUTION TEST CHART
NATIONAL BUREAU OF STANDARDS-1963-A

(12) 5c

AD

(6) The Physical Mechanisms Responsible for the Weathering of Epoxy Resins and GFR Epoxy Resins.

(9) Final Technical Report, Sep 76-Oct 78

by

(10) T. W. Turner
K. H. G. Ashbee

(11) October 1978 (12) 35p.

EUROPEAN RESEARCH OFFICE
United States Army
London England

(15) Grant Number DA-ERO-76-G-068

H. H. Wills Physics Laboratory
University of Bristol

(16) 1T161102BH57 (17) 04.00

Approved for Public Release: distribution unlimited

UNCLASSIFIED

SECURITY CLASSIFICATION OF THIS PAGE (When Data Entered)

REPORT DOCUMENTATION PAGE		READ INSTRUCTIONS BEFORE COMPLETING FORM
1. REPORT NUMBER	2. GOVT ACCESSION NO.	3. RECIPIENT'S CATALOG NUMBER
4. TITLE (and Subtitle) The Physical Mechanisms Responsible for the Weathering of Epoxy Resins and GFR Epoxy Resins		5. TYPE OF REPORT & PERIOD COVERED Final Technical Report September 76 - October 78 6. PERFORMING ORG. REPORT NUMBER
7. AUTHOR(s) T.W. Turner K.H.G. Ashbee		8. CONTRACT OR GRANT NUMBER(s) DAERO-76-G-068 ✓
9. PERFORMING ORGANIZATION NAME AND ADDRESS University of Bristol Bristol, U.K.		10. PROGRAM ELEMENT, PROJECT, TASK AREA & WORK UNIT NUMBERS 6.11.02A-1T161102BH57-04 00-598
11. CONTROLLING OFFICE NAME AND ADDRESS U.S. Army R&S Group (EUR) BOX 65 FPO NY 09510		12. REPORT DATE OCTOBER 1978 13. NUMBER OF PAGES 33
14. MONITORING AGENCY NAME & ADDRESS(if different from Controlling Office)		15. SECURITY CLASS. (of this report) UNCLASSIFIED 15a. DECLASSIFICATION/DOWNGRADING SCHEDULE

16. DISTRIBUTION STATEMENT (of this Report)

Approved for Public Release

Distribution Unlimited

17. DISTRIBUTION STATEMENT (of the abstract entered in Block 20, if different from Report)

18. SUPPLEMENTARY NOTES

19. KEY WORDS (Continue on reverse side if necessary and identify by block number)

(U) GRP Epoxies
(U) Water Uptake
(U) Weathering of Epoxies
(U) NDT of Composite

20. ABSTRACT (Continue on reverse side if necessary and identify by block number)

SEE OVER

DD FORM 1 JAN 73 1473 EDITION OF 1 NOV 65 IS OBSOLETE

UNCLASSIFIED

SECURITY CLASSIFICATION OF THIS PAGE (When Data Entered)

Ultrasonic photoelasticity experiments have been used to detect the occurrence of plasticisation of the matrix of polymer matrix composites during water uptake. The experimental programme on steel, soda glass, quartz, epoxy resin system 1009, and a polyester resin composite has now been completed and it has been demonstrated that small changes in bulk properties, such as those resulting from plasticisation caused by water uptake by epoxies, can be detected and distinguished from localised defects such as cavities. The latter are readily identified by the interference patterns which they generate. A program has been developed to give computed images which closely resemble the fringe systems observed experimentally.

A novel experiment, designed to permit precise exploration of the interfacial bond between silica and epoxy resin during water uptake, has been developed. The test-piece takes the form of resin coated single crystal specimens of quartz. By exploiting the piezoelectric effect in crystalline quartz, it is anticipated that mechanical damping by the resin coat will be extremely sensitive to the state of bonding.

In another experiment, dimensional changes which occur in the matrix of fibre reinforced plastics as water is absorbed, are being mapped by measurement of the stress birefringence in the resin between closely packed fibres.

Conclusions are drawn from the work reported herein, and from the work described in the 1st Annual Technical Report, October, 1977.

TABLE OF CONTENTS

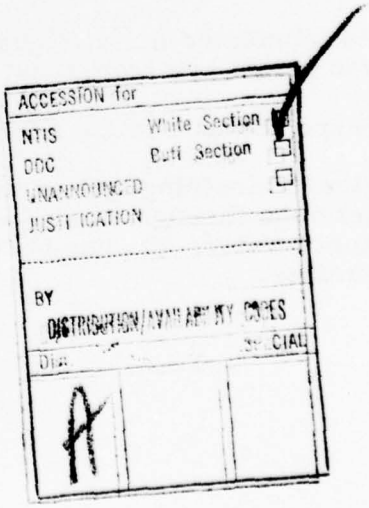

LIST OF FIGURES

1. INTRODUCTION

Three avenues of research have been followed during this reporting period. One concerns the application of photoelastic imaging of ultrasound in order to detect plasticisation of the epoxy resin matrix of composites during water uptake. The successful detection, and identification using computed images, of defects is an added bonus from this part of the work. The second area of research is development of an experiment designed to probe deterioration of the chemical bond between SiO_2 and epoxy resins during water uptake. The specimen is a resin coated single crystal of quartz. It is anticipated that deformations induced by the piezoelectric effect will be sensitive not only to the presence of a resin coating but also to the efficiency of load transfer between crystal and resin. The third topic of investigation has been measurement of changes in stress in the resin that arise from the differential contraction between resin and fibre material during cooling from the cure temperature but which change as a consequence of resin swelling during water uptake.

2. ULTRASONIC PROTOELASTICITY

2.1 COMPUTER MODEL

Good agreement from a computer model with schlieren experiments for the interaction between an ultrasonic pulse and a surface defect in a pipe, has been obtained by Slater el al[1]. They envisage a series of radiating poles along the defect, and apply ray theory to obtain fringe patterns from 18 rays. This number arises from the three rays assumed to strike the defect, namely the direct ray, that reflected at an interface with mode conversion, and the reflected ray without mode conversion. Since each of these takes the form of two rays, the incident radiation comprises six rays, viz three longitudinal and three shear. Hence there are 18 paths by which the 6 incident rays return to the observed point. This model is not suitable for the photoelasticity images reported here since there are no circumstances where 18 rays can be observed simultaneously because the Transistor Transistor Logic (TTL) control of the L.E.D. restricts the number of fringes observed, i.e. the number of interferences observed, to between one and twenty-five by means of the enabling pulse.

Another drawback with the model used by Slater et al is that the use of radiating poles on the defect is expected to introduce some granular effect in the output, particularly for small defects. This problem is avoided here by treating the defect as a continuous reflector. An added advantage of this concept is that a very small region in the 'visualised' zone can be examined in detail.

Figure 1 shows the configuration used for the present work. It is assumed that:

1. the transducer, OT, is made up of a series of equally spaced point sound generators,

2. the defect is perfectly round, shown as a semi-circle on the centre line OX because of symmetry,

3. the 'visualised' region ABCD is made up of a matrix of points, P, an array 31 x 31, chosen to conform with the computer graphics, a step of 0.5 mm covering a region 1.5 x 1.5 cm,

4. the acoustic impedances of opaque and transparent material are the same,

For any point, P, there is a path which, emanating from T, is reflected from the defect such that:

$$90 - \theta - \varphi = \theta + \psi \qquad (1)$$

This condition is satisfied when

$$\tan (2\theta + \varphi) = \frac{y - r \cos \theta}{x - a + r \sin \theta} \qquad (2)$$

Eliminating φ, we have:

$$2 \tan\theta\,(a x + b y - a^2) - r(1 + \tan^2\theta)\{(y + b)\sin\theta + (x - 2a)\cos\theta\} + (1 - \tan^2\theta)\{b x - a y - a b\} = 0 \quad (3)$$

This equation can be solved numerically to find a value of θ; convergence is rapid, thus an accurate path length can be found from which the attenuation factor, inversely proportional to the square of the path length, and the phase at point P may be determined.

Numerical solution of equation 3 above relates to a wave which is not mode converted on reflection. For the situation where a longitudinal wave is mode converted to a shear wave we have

$$\frac{\sin(90 - \theta - \varphi)}{\sin(\theta + \psi)} = \frac{C_L}{C_T} = r_c \quad (4)$$

where C_L is the velocity of the longitudinal wave and C_T is the velocity of the transverse wave, and from which we obtain

$$\tan\theta = \frac{\cos\varphi - r_c \sin\psi}{\sin\varphi + r_c \cos\psi} \quad (5)$$

φ can be expressed in terms of θ since

$$\tan\psi = \frac{x - a + r\sin\theta}{y - r\cos\theta} \quad (6)$$

$$\text{and } \tan\phi = \frac{b - r\cos\theta}{a - r\sin\theta} \quad (7)$$

Combination of equations (5), (6) and (7) will give an expression for θ comparable with equation (3), both ψ and φ having been eliminated. This is, however, both tedious and unnecessary. Numerical methods applied to equation (3) indicate a rapid convergence, and there is no reason to suppose that changing r_c from unity (the situation in equation (3)) to 1.5846 (the ratio of velocities in fused quartz) should alter the convergence very significantly. This has been found to be true; any value assigned to θ enabled ψ and φ to be evaluated from equations (6) and (7). These values can then be used in (5) to obtain a new value for θ. Typically, 10 iterations give a value of $\theta \pm 1 \times 10^{-5}$ radians. The tolerance value used in the program is 10^{-3} radians, yielding a reflection point accuracy better than $\lambda_T/500$.

With θ precisely known, the longitudinal path length is accurately computed from

$$\{a^2 + b^2 + r^2 - 2 a r \sin\theta - 2 b r \cos\theta\}^{\frac{1}{2}} \quad (8)$$

and the shear wave path length from

$$\{(x-a)^2 + y^2 + r^2 + 2(x - a) r \sin\theta - 2 y r \cos\theta\}^{\frac{1}{2}} \quad (9)$$

The program so far has been written to evaluate a 'pressure' in the 'visualised' matrix, setting phase α to 'pressure', for a particular value of b, (point source transducer) and includes the direct shear wave 'pressure' from the transducer where the path length is

$$\{(y - b)^2 + x^2\}^{\frac{1}{2}} \qquad (10)$$

The procedure is repeated for the next value of b, and continued until the whole 'transducer' has been constructed.

Figure 2(b) shows a photograph where the squared region represents the area 'visualised' in the computer program. The hole size is 1 mm radius and the ultrasonic frequency 2.0 MH_z.

Figure 3 shows a Symap* representation of the area. This represents the maximum number of shadings available, therefore a new program was written with assistance from A. Brown[2] to allow up to 100 shadings, see Figure 4. 'Totally black' still covers only about a quarter of the area, and the representation is not satisfactory. Symvu, Figure 5, shows a contour map where the maximum pressure is represented by a height of 3", with a minimum of 0". Figures 6 and 7 are similar with the azimuth rotated round from 0^o to 25^o and 335^o respectively.

2.2. PHOTOELASTIC EXPERIMENTS

Detailed descriptions of the apparatus and experimental method were given in the annual technical report, October 1977. The experimental work since that date has been primarily concerned with the accuracy to which longitudinal and shear wave velocities may be measured. An attempt was made to prepare stress-free specimens with a view to observing photoelastic images in the resin itself, and especially in the vicinity of a fibre. However, the stress field generated by resin shrinkage during curing was always substantial and effectively obliterated any fringes resulting from the ultrasound. To circumvent this difficulty, it was decided to "collect" data from a stressed and even opaque specimen and "read" the information in an adjacent visualising block, the specimen and block being acoustically coupled. The TTL control employed here is particularly suitable for precise timing and since the experiments can be designed so that timing is done differentially, great accuracy is possible.

---

* SYMAP is a computer program for producing maps which graphically depict spacially disposed quantitative and qualitative information. SYMAP was designed and developed by the Laboratory for Computer Graphics at Harvard University, U.S.A.

The transducer which has been designed and developed in the laboratory, produces both longitudinal and shear waves but, for measurements from a single fringe, well defined shear pulses, generated by mode conversion from a longitudinal pulse that is incident on a vertical glass/air interface, were used. The transducer is simply a piezoelectric device placed on top of a small block of soda glass shown in Figure 8. When a specimen of known thickness is placed between the soda glass and the quartz visualising block, it takes longer for the pulse to reach a given point by an amount that is determined by plotting fringe position in the quartz against the time taken to reach that point. Two plots are required, one with and one without the specimen in position. An arbitrary zero is chosen to give the sample transit time, from which both longitudinal and shear wave velocities may be determined. For isotropic materials:

$$E = 2(1+\nu)\rho C_T^2 = \frac{(1+\nu)(1-2\nu)\rho C_L^2}{(1-\nu)}$$

$$\nu = \frac{\frac{1}{2}\left(\frac{C_L}{C_T}\right)^2 - 1}{\left(\frac{C_L}{C_T}\right)^2 - 1} \qquad G = \rho C_T^2$$

where E and G are the elastic moduli, ν is Poisson's ratio, and C_T and C_L the transverse and longitudinal wave velocities.

For anisotropic materials and particularly composites, the situation is made complex, and the elastic constants can only be relevant in directions where the material is uniform. However it is possible to obtain the delay time which a wave takes to cross a known dimension of a 90^o cross-ply woven rovings glass fibre reinforced resin and thus an average velocity is found. Experiments have shown that these average velocities are sensitive to water uptake.

Measurements were taken using a horizontal grid for the longitudinal waves at normal incidence to the sample and visualising block. The reflected shear pulse makes an angle θ with the vertical (See Figure 9) in the soda glass and ψ in the quartz. θ and ψ are readily calculated from the known optical properties of the soda glass and quartz and the measuring grid was arranged to be perpendicular to the direction of propagation.

A series of experiments has been completed on specimens of steel, soda glass, quartz, epoxy resin system 1009 both before and after water uptake, on a polyester resin composite containing 67% E. glass woven rovings and on cured and uncured samples of CIBA-GEIGY MY 750 DGEBA resin.

When the ultrasound passes normally through the specimen its velocity is easily found since the distance travelled and time taken are known. For oblique incidence, the direction taken through the soda glass and that through the quartz need to be determined in order to use the equation:

$$C = \frac{X}{\cos \phi} \left\{ \frac{1}{T + \frac{x \tan \phi \sin \theta}{C_{L1}}} \right\}$$

where C_{L1} is the velocity of shear waves in soda glass

X is the specimen thickness.

The time at which the ultrasound wave is visualised after leaving the transducer is variable and can now be measured accurately with a Racal timer. For each fringe setting, the spatial position is located on a grid. Ten readings of the delay time were averaged to build up the distance-time curve. Linear regression analysis was used for each data set, so that the time delay for each sample at the chosen arbitrary origin could be obtained.

An estimation of the random errors has been made using standard statistical procedures. There is a systematic error caused by the time taken for the fringe to cross the interfacial layers: differential methods cannot be applied when measurements with the specimen in situ involve an extra interface. However it does appear that the total error is somewhat less than 0.5% as the longitudinal and shear velocities for quartz show:

$$C_L = 5.938 \pm 0.025 \times 10^3 \text{ m/s}$$

$$C_T = 3.746 \pm 0.013 \times 10^3 \text{ m/s}$$

Such results compare very favourably with those obtained from the standard Pulse Echo Overlap (P.E.O) technique, but it should be pointed out that the values shown above are obtained from averaging almost 100 separate data sets, such a quantity of data being available because each test (whatever the specimen material) automatically generates data sets for quartz. Results for all the specimens are given in Table 1. The curing schedule used for the 1009 epoxy samples was gelling at 90° C for 12 hours followed by a 4 hour cure at 177°C. A value for the velocity of what was believed to be the shear wave was obtained at oblique incidence, but at 2,716 ± 85 m/s it is clearly longitudinal wave velocity. The P.E.O. measurements demonstrate that shear waves in epoxy samples are highly attenuated and hence are difficult to detect photoelastically. Correct identification of the fringes is facilitated in the multiple flashing mode because the shorter wavelength of the transverse waves is prominent. Incorrect identification arises when a single pulse, often more easily measured, is being visualised.

	C_T m/s	C_L m/s	ν	G GN/m^2	E GN/m^2
Quartz	3,746 ± 13	5,938 ± 25	0.169 ± .008	30.9	72.3
Quartz (P.E.O)	3,767	5,935	0.163		
Steel	3,201 ± 44	5,815 ± 32	0.282 ± .009	80.7	207
Steel (P.E.O)	3,183	5,939	0.298		
1009	(see text)	2,795 ± 10			

Table 1

Ultrasonic velocity measurement with computed elastic constants.

The longitudinal velocity against boiling time for the cured and uncured MY 750 epoxy resin samples are shown in Figure 10 with density curves in Figure 11. The bars represent the tolerance range for each velocity measured. The shear wave curve is missing because of the high attenuation associated with the transverse wave. More comprehensive data are available for two GRP samples. Figure 12 shows the longitudinal and shear velocities plotted against the immersion time in boiling distilled water, with thickness and weight changes in Figures 13 and 14.

The critical stage of water damage arises when water diffuses along the resin/glass interface. Detection of this water at the interface itself has not been achieved using ultrasound of a few megacycles; it is anticipated that a frequency increase of two orders of magnitude would be required. The frequencies used here are capable of revealing changes in the bulk properties. Water uptake by 'wicking' (capillary flow along the interface) is almost certainly completed before the first minimum in the curves of Figure 12. Thus debonding is clearly linked to the initial drop in the measured ultrasonic velocities, < 10 hours. There is also an expected initial rise in the velocities due to closure of interfacial gaps under the action of stressing during assembly of the apparatus. Post curing and plasticisation during exposure to water at $100^{o}C$ are also expected to affect the velocities. The occurrence of these phenomena during the first 30 hours is also resolved by the thickness measurements (Figure 13).

The much slower diffusion through the resin bulk (than along resin/fibre interfaces) introduces a lowering of the modulus and a reduced velocity in the outer layers. As time proceeds, the relation signs of the soft outer shell and the hard inner core will change causing changes in the self-stress field arising from water uptake. The release of internal stresses is accompanied by a significant steep drop in the ultrasonic velocities (~ 120 hours) implying a considerable reduction in the elastic moduli. The steady increase in velocity after 120 hours is attributed to the leaching of low molecular weight material from the resin. It will be noted in the Figures that the somewhat thicker specimen B of GRP has apparently not yet reached saturation after 120 hours exposure to boiling water.

3. EXPLOITATION OF THE PIEZOELECTRIC EFFECT IN CRYSTALLINE QUARTZ IN ORDER TO DIRECTLY MEASURE DEGRADATION OF LOAD TRANSFER AT SiO_2/RESIN INTERFACES.

Assuming that the chemical bonding between glass fibres and epoxy resins is reproduced at interfaces between crystalline modifications of silica and the same resins, a resin coated single crystal quartz test-piece has been developed in order to investigate the effects of water uptake by the resin on deformations resulting from the piezoelastic effect in the quartz but influenced by the strength of the SiO_2/epoxy bond. In order to magnify the mechanical displacements and hence facilitate their accurate measurement, it was decided to fabricate helical springs from quartz single crystals; a small twist in the helical element manifests itself by a much larger axial displacement of the helix.

A large natural single crystal weighing almost 650 grams was waxed on to a 3/8 inch thick block of plate glass and this was subsequently mounted to the removable brass plate that is mechanically attached to the two-circle goniometer of a "Capco" Q-35 annular saw. The crystal was oriented by transfering the goniometer to an X-ray set, and then cut into basal slabs measuring 2 cm in thickness.

Specimen fabrication involves shaping the basal slabs into helices using diamond impregnated tools on an ultrasonic milling machine. The first machining operation is tube-boring of concentric c-axis tubes having $O/_D$ 9.0 mm, 14.7 mm and 20.0 mm respectively, and nominal wall thickness 2.6 mm. To support the material during this operation, each slab is first mounted onto a glass block. The crystallographic a-directions are scribed on the slab. The core drills were supplied by Impregnated Diamond Products Ltd., Gloucester.

Each tube is then bonded to the inside of a protective glass sleeve and fabricated into a helix (having three evenly spaced turns of 2.6 mm x 1.43 mm section and 3.2 mm pitch, and a 3.6 mm length of plain tube at its ends) by mounting the tube onto a glass mandrel which is clamped to a lead screw and presented at the helix angle ($\sim 5^{o}$) to a horizontal cutting wheel. The glass sleeve prevent the incidence of surface chipping on the quartz helix. The helix cutting attachment bolts to the table of the milling machine. The general layout is shown in figure 15 and the close-up view of the helix cutting attachment is shown in figure 16. Figure 17 shows an as-cut helix which is unetched, having pitch 3 mm, thread thickness 2.4 mm and thread width 1.6 mm.

The lead screw of the helix cutting attachment has pitch (3 mm) equal to that required of the helix and is driven via the key-way of a shaft which is itself driven through a single worm reduction gear box (100:1 ratio). The combined axial and rotational motions generate a helix when the specimen tube blank, fitted as an extension of the spindle, contacts the saw blade. The edge of the blade is impregnated with diamonds and was also supplied by IDP.

To start cutting, the spindle is fully retracted and the required outer limit of the cut is positioned to just contact the rim of the diamond saw. With the milling machine switched on, a superficial mark is made adjacent to one of the crystallographic a - directions and the machine table is advanced horizontally by 4.2 mm so that a cut is made which exactly corresponds to the required inter-turn spacing.

The finished helix is gently removed from the mandrel assembly after softening the lakeside cement used as mounting medium by soaking overnight in chloroform at room temperature. Any surface flaws introduced during fabrication are removed by etching each specimen for 30 minutes in a 20% fresh hydrofluoric solution at room temperature. Subsequent handling of the specimen is done with rubber tipped tweezers.

At the time of writing this report, experiments were under way to optimise a technique for evenly coating the quartz helices with epoxy resin.

4. THE STRESS FIELD ARISING FROM THE INHOMOGENEOUS SWELLING OF THE RESIN FILLET CONTAINED BETWEEN CLOSELY PACKED FIBRES.

The resin swelling that accommodates water uptake by fibre reinforced plastics is larger near to than it is remote from the external surface. As a consequence, the fillet of resin between three close packed fibres (Figure 18A) would, if unconstrained by the presence of fibres, undergo the shape change illustrated in Figure 18 (B). The concentration of water eventually reaches saturation in the resin adjacent to the external surface and a region of saturated swelling begins to move inwards as indicated in Figure 18 (C). However, the resin is not free to adopt these shape changes. The fibres are not able to conform to the above changes in profile and, as a result, the swollen resin experiences radial compression and, correspondingly, the unswollen resin experiences radial tension. By preparing 3 mm thick transverse sections through a unidirectional composite which has been exposed to hot water, a preliminary examination has been made of the stress birefringence in the fillet of resin between three closely packed fibres, Figure 19; the numbers in Figure 19 denote distance (mm) from the external surface.

The range of birefringence resolved in Figure 19 is large, ranging from grey to red on the Michel-Levy chart. This, coupled with the fact that the stress-optical coefficient is small for epoxy resins, indicates the presence of very high stresses (probably a few tens of MN/m^2). Since diffused water will undoubtedly migrate towards the tensile part of the stress field, i.e. towards the middle of the fillet of resin, analysis of the stress field and measurement of the anticipated self-stress enhancement of water migration are fundamental to the problem of weathering of composite materials.

Much of the birefringence of special interest in figure 19 is small, being within the grey region of the Michel-Levy chart. Also, changes in magnitude of the birefringence occur in distances of the order of the limit of resolution of conventional light microscopes ($\sim 0.2\ \mu m$). Hence, to fully investigate the state of stress arising from the strongly inhomogeneous nature of water uptake by the resin between fibres in composite materials, superior polarising optics are essential. Optics meeting our requirements have been developed (for biological research) - for use with the Nikon "Apophot" microscope. The system is known as Nikon rectified optics and is described in the brochure 8360 - 01 KEC 410 - 2/1. An application for a grant to purchase this equipment has been made to the Science Research Council (SRC Appln. No. GR-A 8261.1).

The shoulder between fully saturated and less than fully saturated swelling, and the point at which the radial stress changes sign are both very well defined. By observing the locations of each in composites which have been exposed to the same aqueous environment but for different times, it will be possible to measure the rate at which saturated resin swelling penetrates into real composites and the rate at which the associated stress field builds up.

5. CONCLUSIONS

Work carried out during the two years of tenure of this grant has contributed to an increase in understanding of the characteristics peculiar to epoxy resins which renders them susceptible to attack by water. Photoelasticity experiments, visualising ultrasound, has been demonstrated to be an effective method for observing the bulk behaviours of simple single phase specimens and of two-phase glass/resin composites. Single phase specimens can be investigated for localised defects since defects generate well defined interference patterns which can be simulated in a computer model. Results from experiments on composites show some sensitivity in correlating the longitudinal and shear wave ultrasonic velocities with plasticisation resulting from water uptake, and there is evidence to suggest that greater sensitivity could be realised with higher ultrasonic frequencies. Counterveiling this is a decrease in sensitivity resulting from an increase in the attenuation of the sound as the frequency goes up, to which must be added a significant attenuation of the shear (or transverse) wave. It is concluded that the photoelastic technique is an attractive diagnostic tool. From the operative point of view, the main attraction is that examination can proceed by visual scrutiny.

It has become increasingly clear during this research period, that a more complete understanding of loss of load transfer ability, i.e. of breakdown of the interfacial bond if there is one, requires detailed microscopic measurement of the stress field close to individual fibres. Such thinking has led to the development of two new techniques for probing the silica/resin interface.

Improved and extended life from epoxy resin composites, in atmospheres rendered hostile by water content, can be achieved by producing chemically pure resins in which no manufacturing residues remain. Thorough characterisation of all the materials, precise stoichiometric resin mixes and precisely established cure schedules are evidently very important. So too is the need to avoid contamination during lay-up and here the desirability of using controlled atmospheres is worth assessing. The efficiency of so-called "coupling agents" and the mechanisms by which they work still require assessment by independent research.

REFERENCES

1. Slater, E.A., Baborovsky, V.M., and March, D.M. 1975, Proceedings of the Ultrasonics International Conference.

2. Brown, A., private communication.

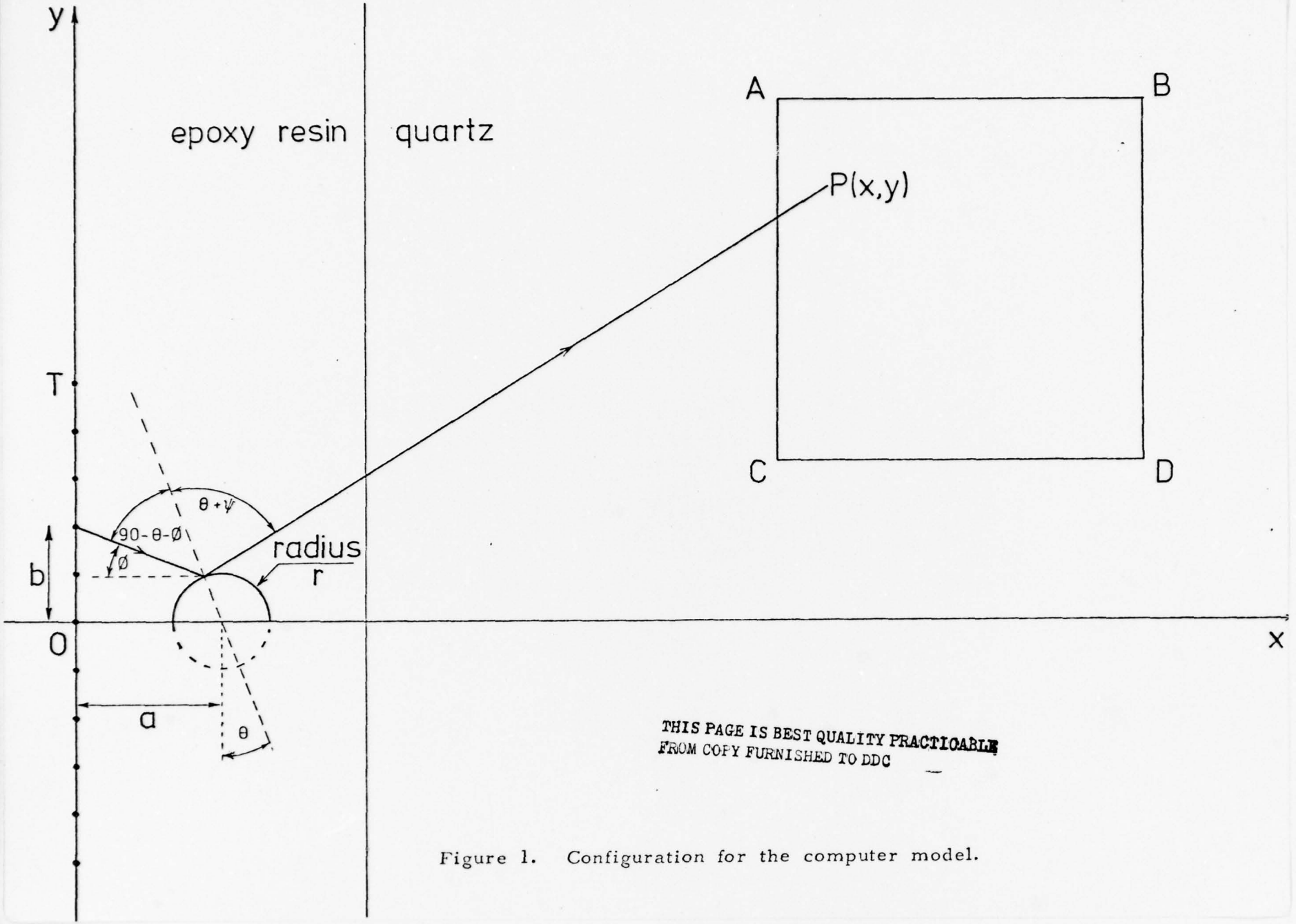

Figure 1. Configuration for the computer model.

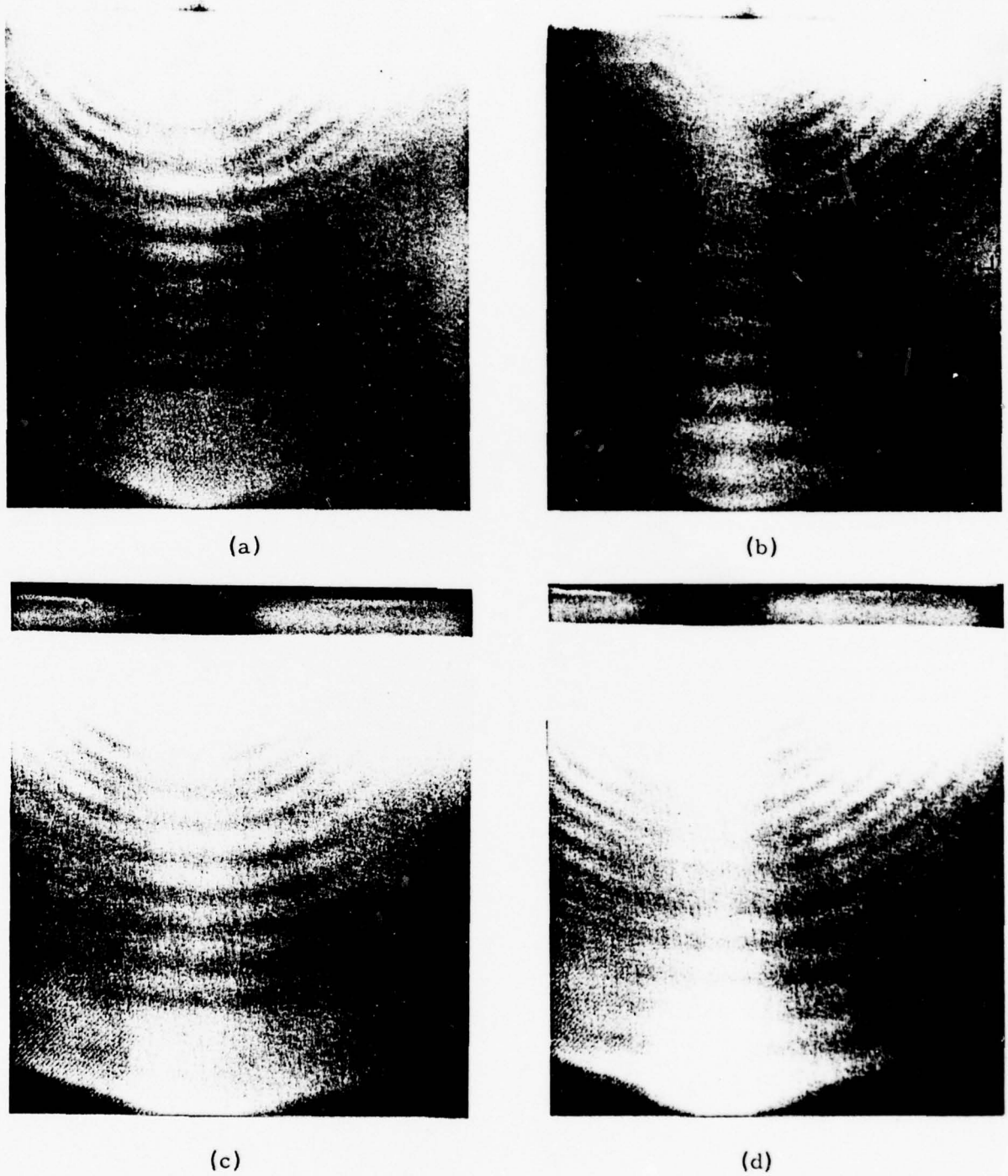

Figure 2. Shear waves reflected from a 2 mm diameter hole in 1009 (a) and (b) with air/epoxy interface. (c) and (d) with water filling the hole.

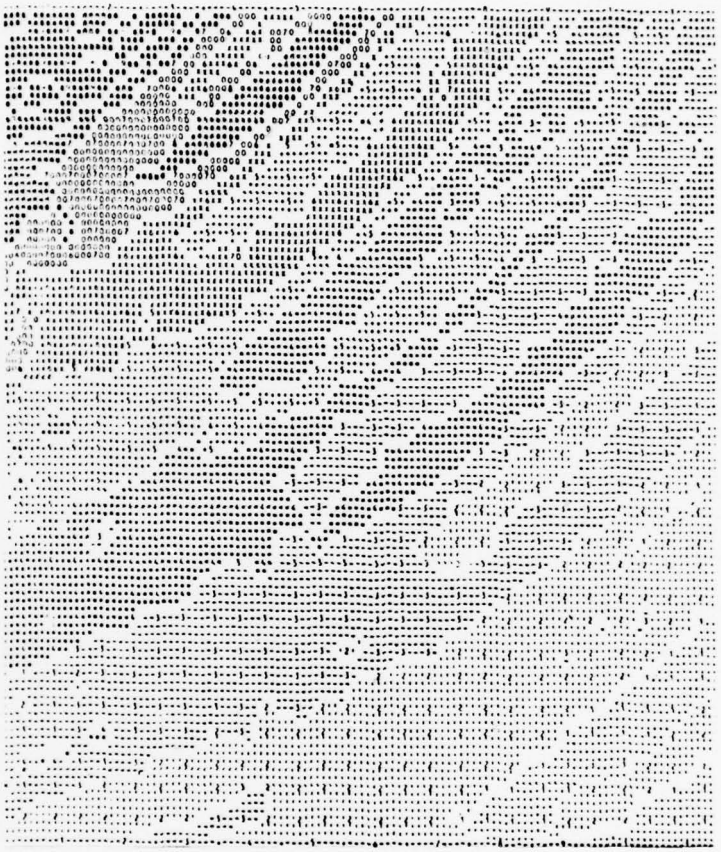

Figure 3. SYMAP representation of shear wave interaction caused by a defect in 1009 resin

0.1 cm hole radius, a = 0.3 cm

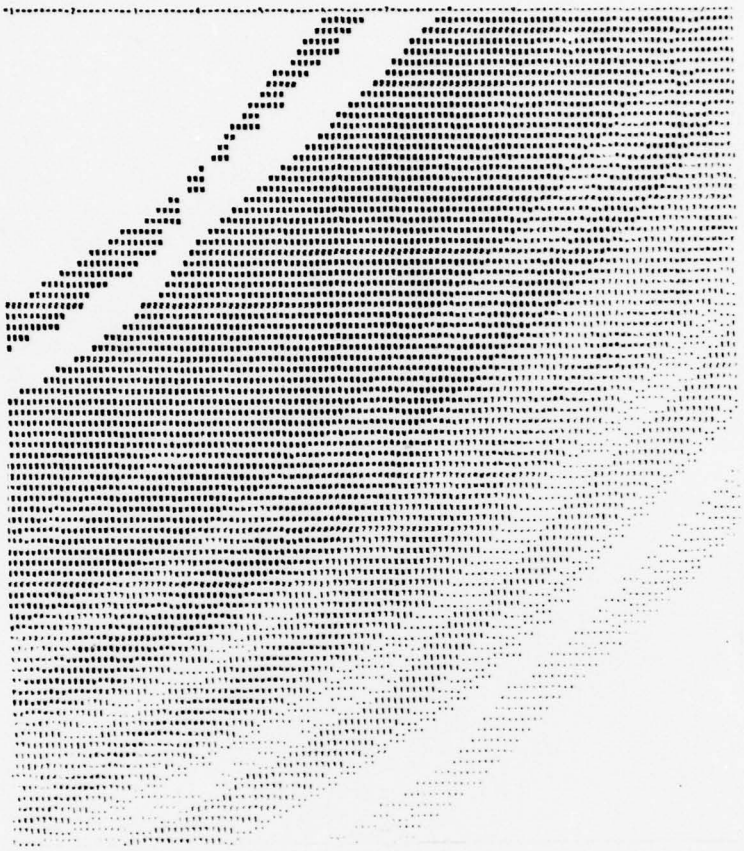

Figure 4. Representation as in Figure 3 with 5 blank - 16 shadings - 19 blank.

N. B. Although 100 shadings can be accommodated in the program, only about 16 can be used effectively in the line printer plot above. To improve the contrast, there are five blank levels in the lower right corner and nineteen shadings left blank at the top.

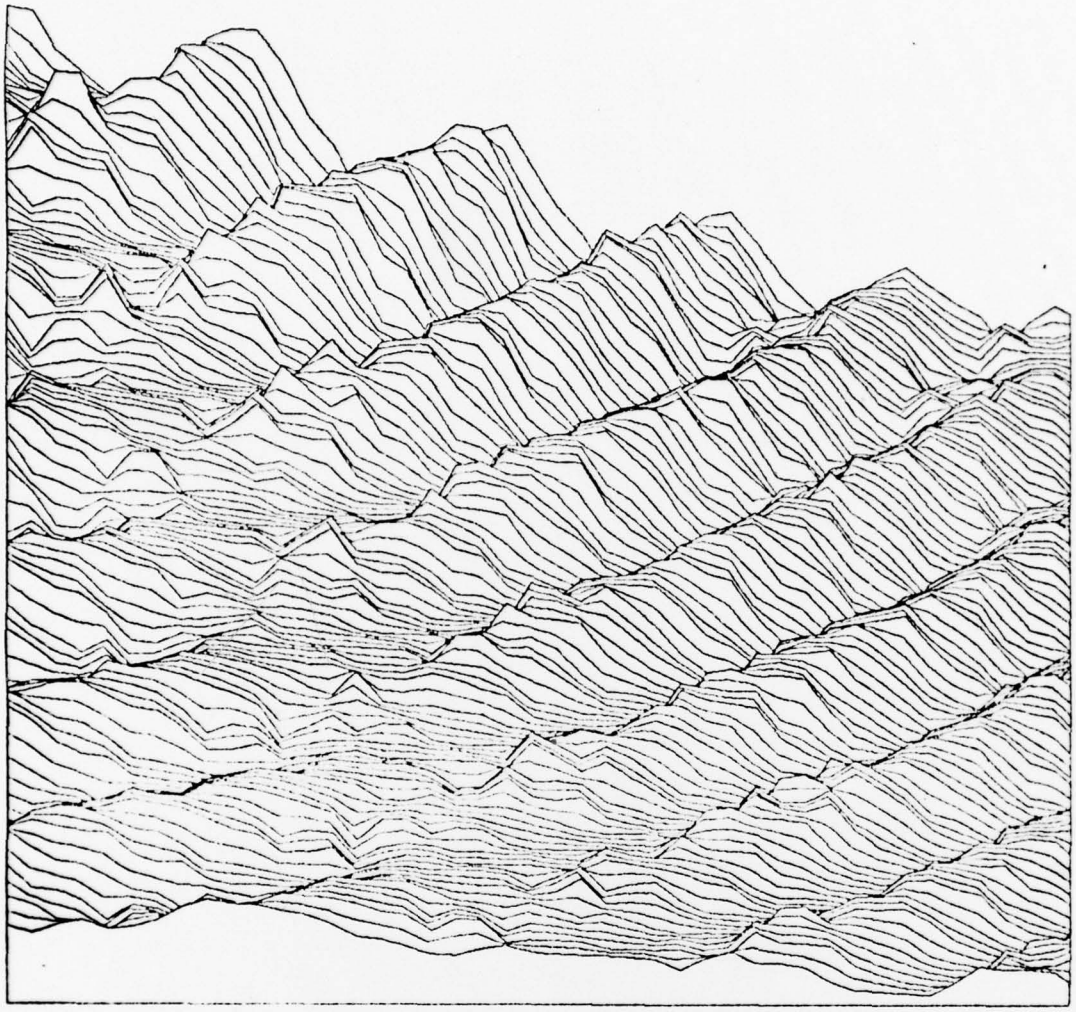

AZIMUTH - 0.00000 ALTITUDE - 30.000
*WIDTH - 6.0000 *HEIGHT - 3.0000

* = BEFORE FORESHORTENING

SHEAR WAVE INTERACTION WITH DEFECT

Figure 5. SYMVU representation for 1009 resin

0.1 cm hole radius, a = 0.3 cm

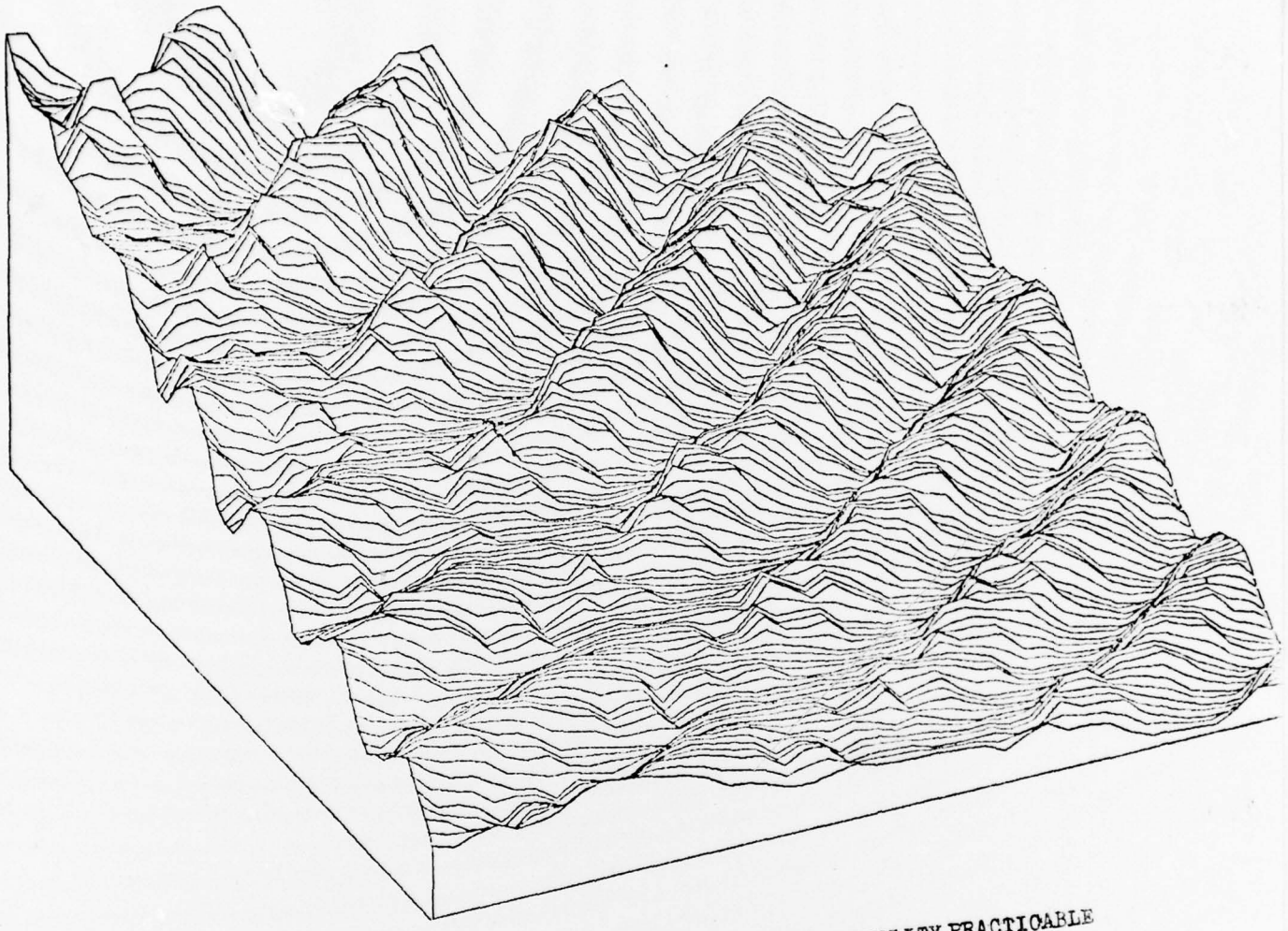

AZIMUTH - 25.000 ALTITUDE - 30.000
*WIDTH - 6.0000 *HEIGHT - 3.0000

* = BEFORE FORESHORTENING

SHEAR WAVE INTERACTION WITH DEFECT

Figure 6. SYMVU representation for 1009 resin

0.1 cm hole radius, a = 0.3 cm

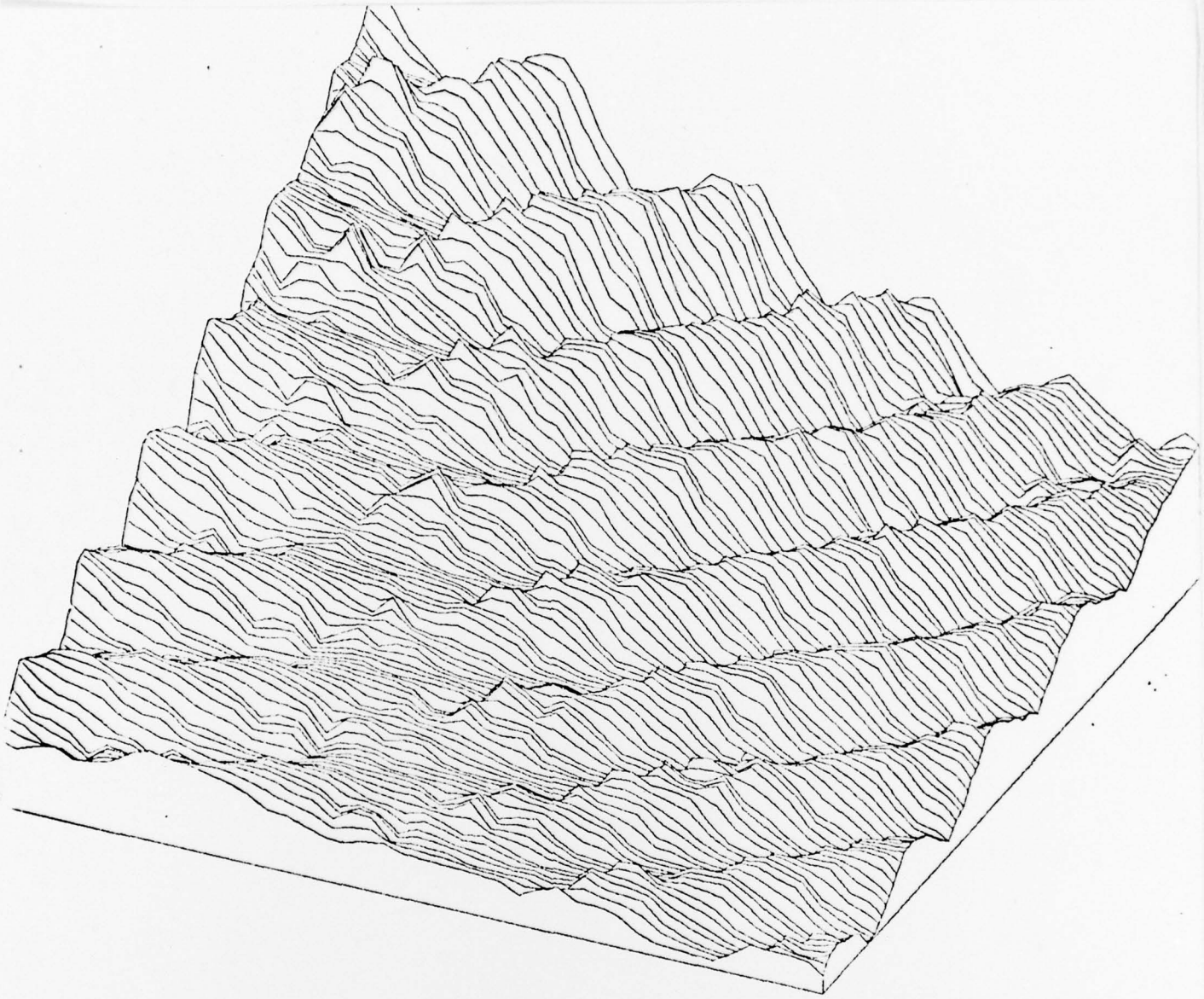

AZIMUTH = 335.00 ALTITUDE = 30.000
WIDTH = 6.0000 HEIGHT = 3.0000

BEFORE FORESHORTENING

SHEAR WAVE INTERACTION WITH DEFECT

Figure 7. SYMVU representation for 1009 resin

0.1 cm hole radius, a = 0.3 cm

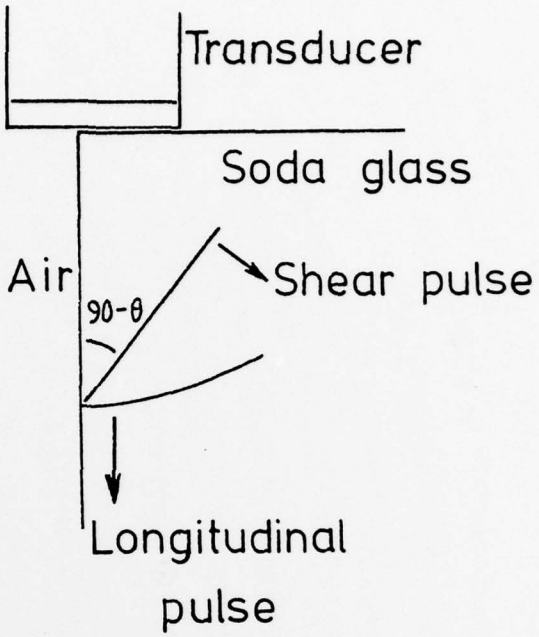

Figure 8 Transducer with glass reflector.

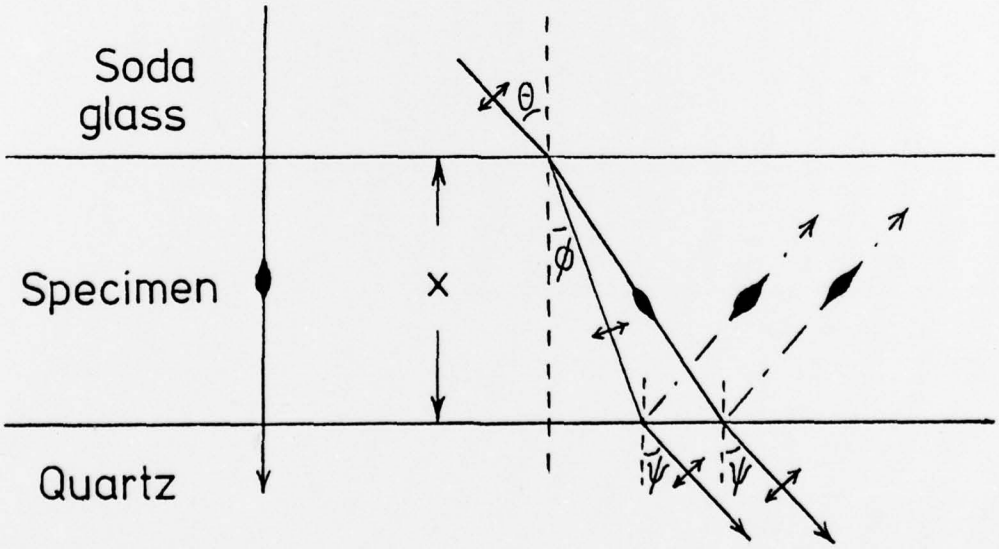

Figure 9 Shear wave progress through specimen.

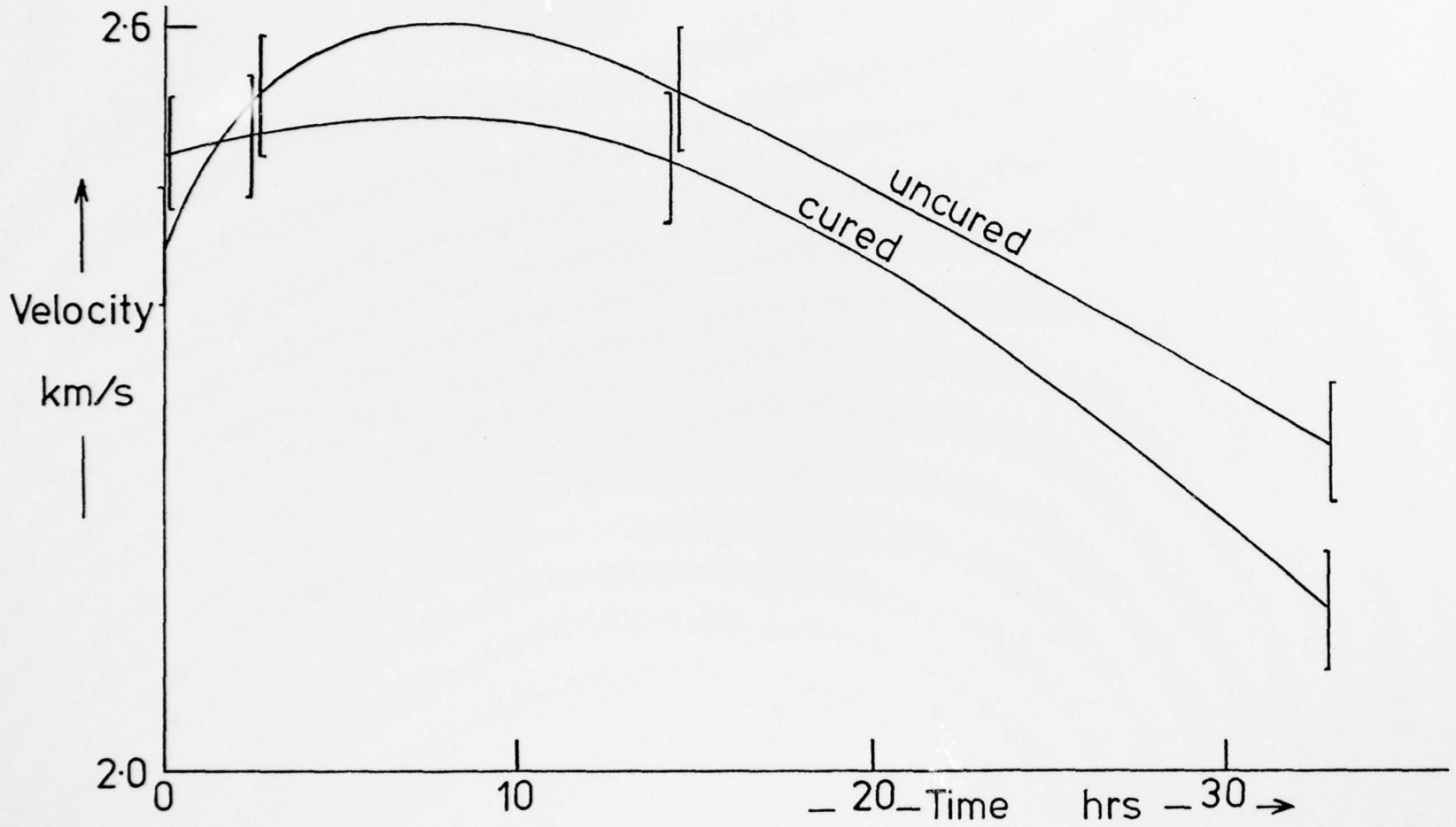

Figure 10. Longitudinal velocity against boiling time for MY 750 resin

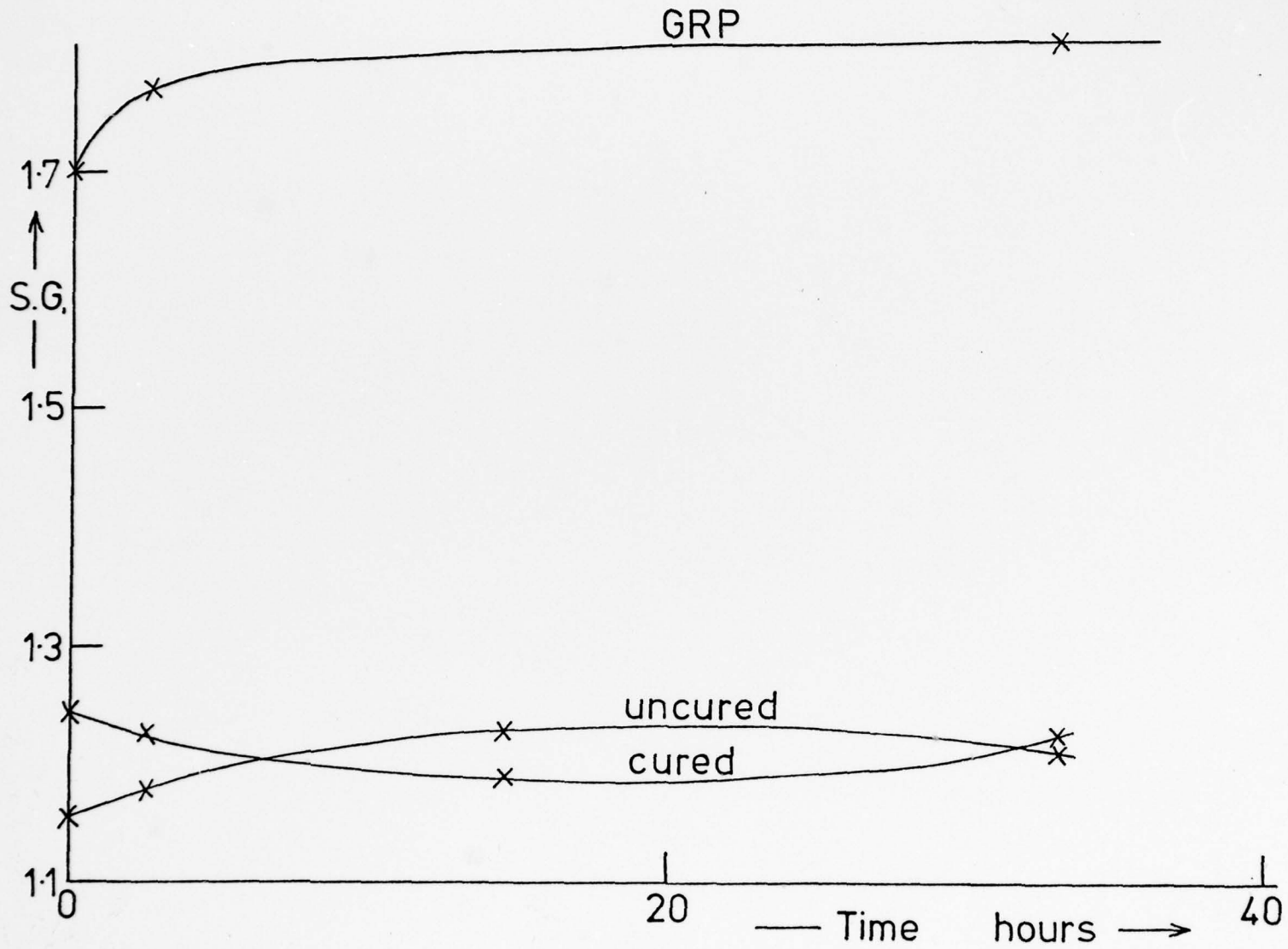

Figure 11. Density against boiling time for resin & GRP

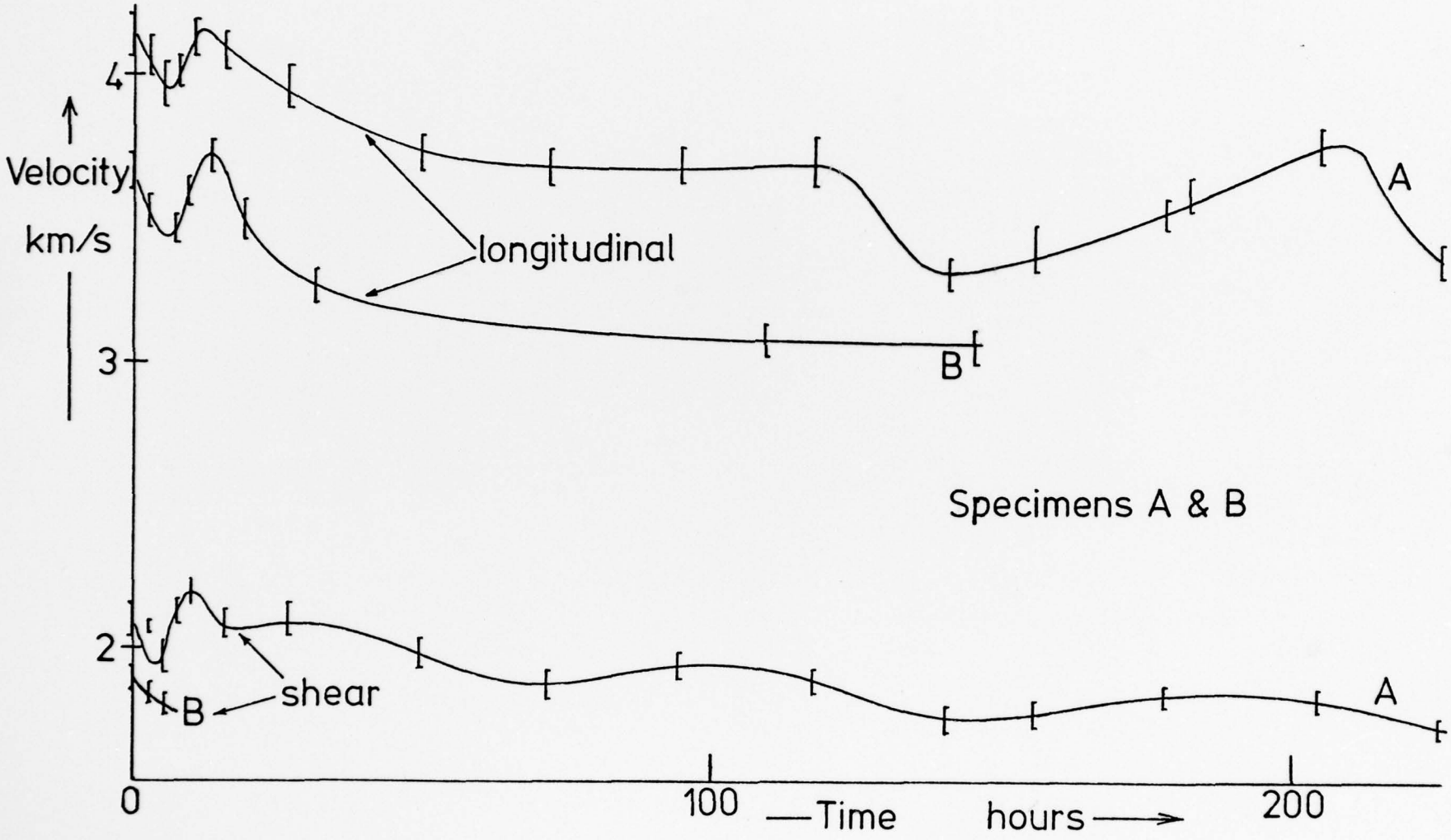

Figure 12. Longitudinal and Shear Velocity against boiling time for GRP

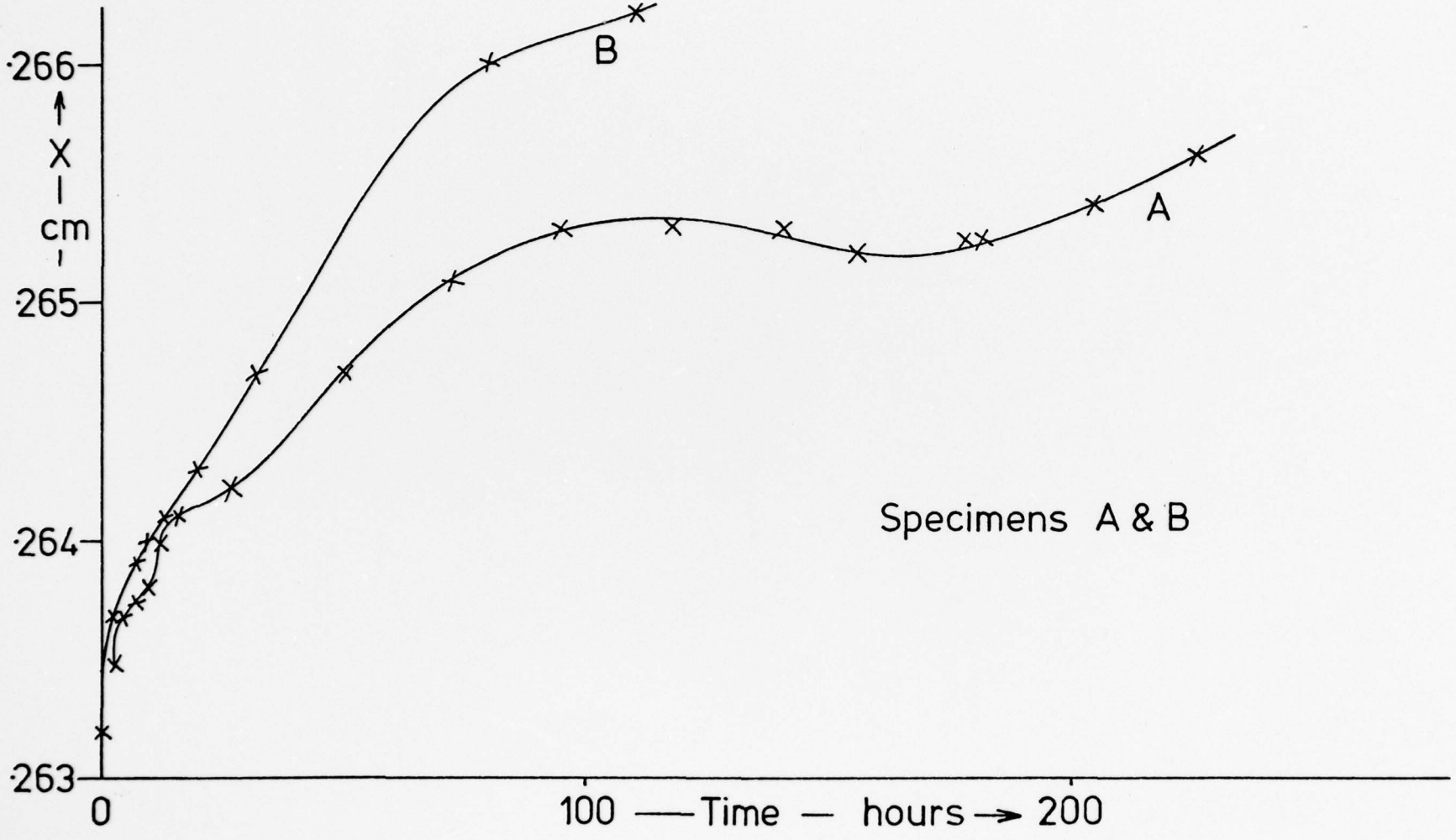

Figure 13. Thickness (sample) against boiling time for GRP

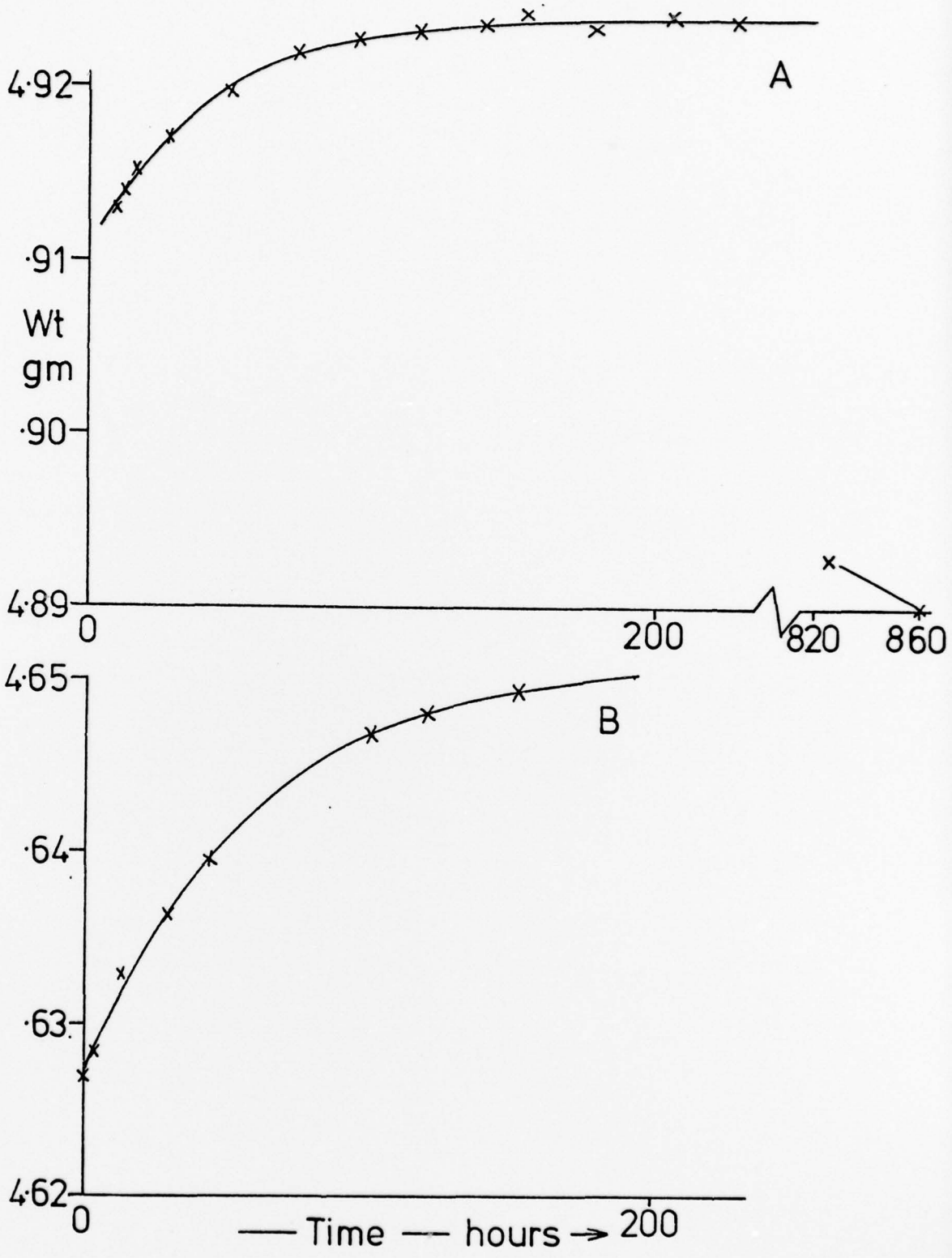

Figure 14. Weight of GRP against boiling time for specimens A & B

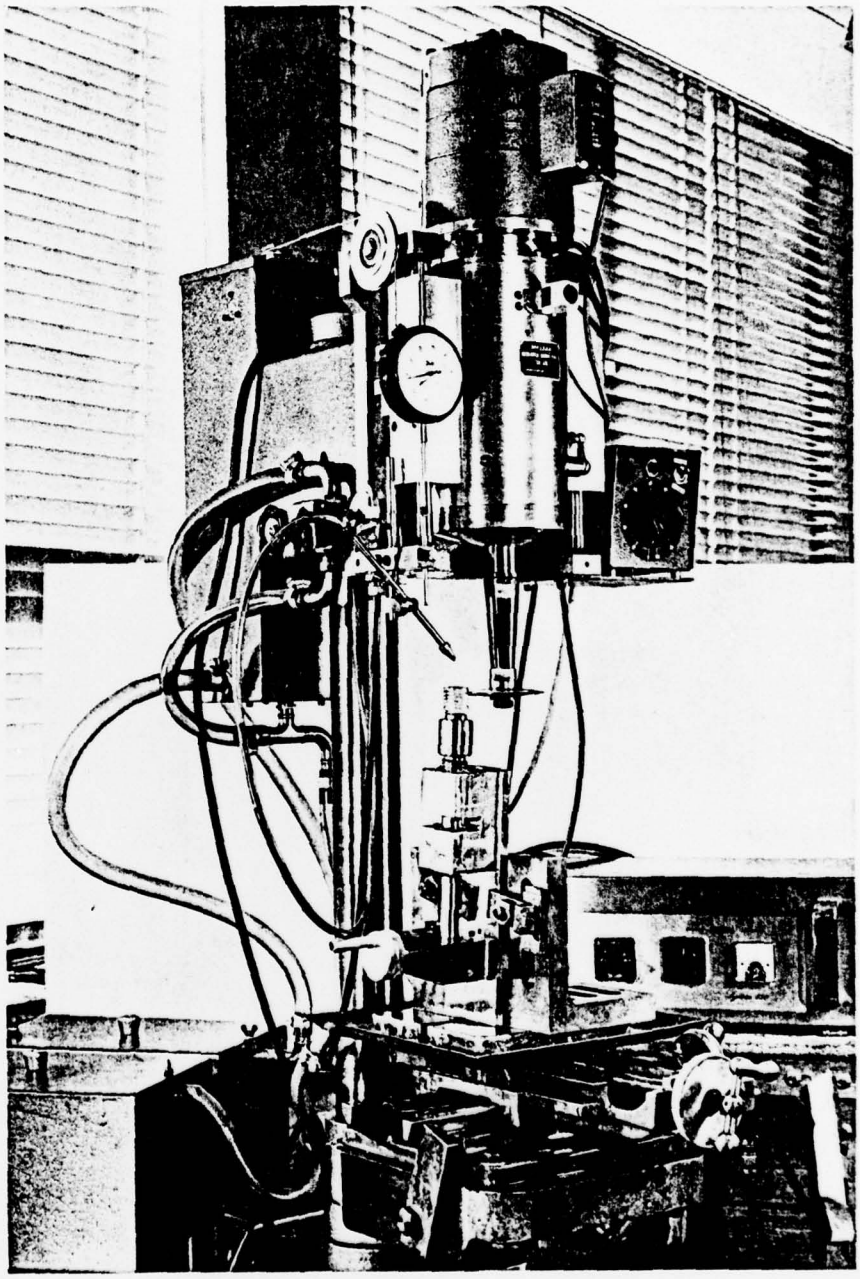

Figure 15. Layout of milling machine used for cutting the helical springs.

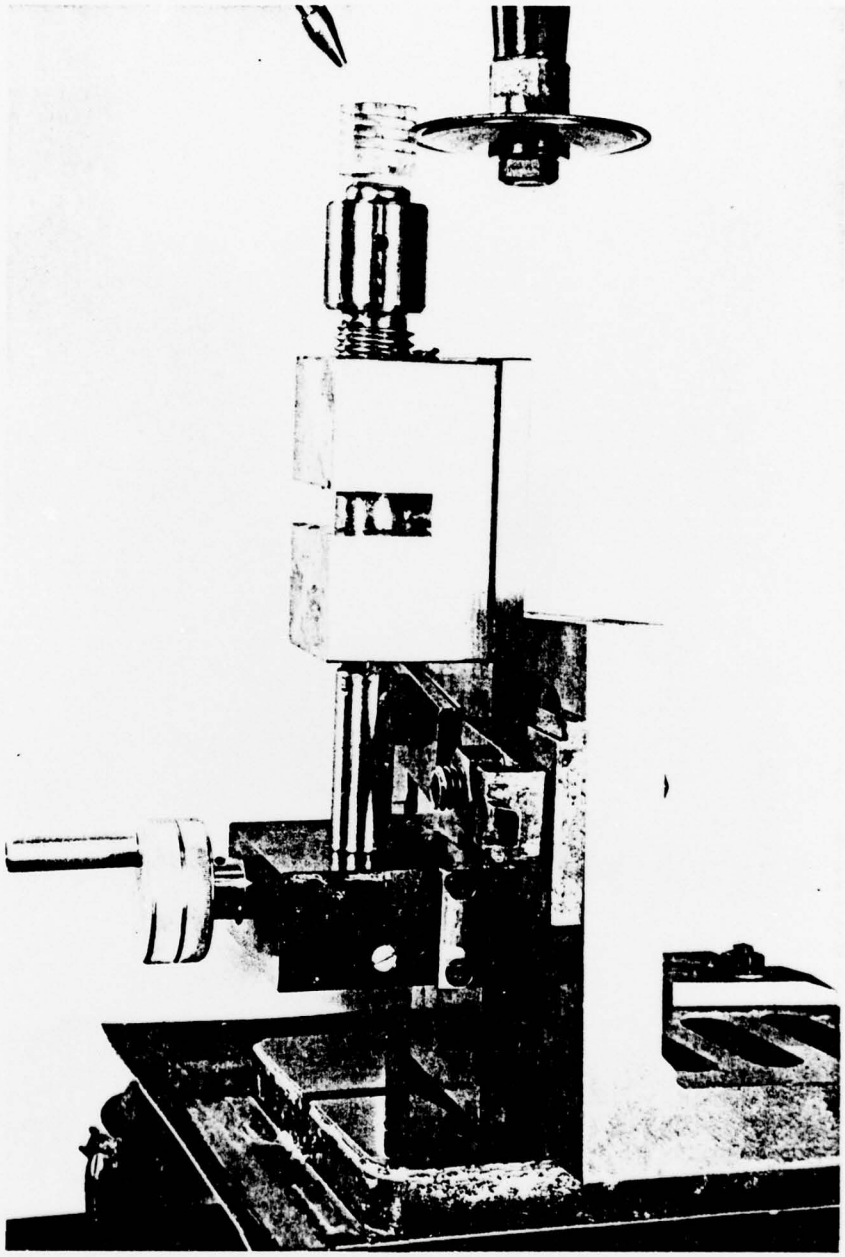

Figure 16. Helix cutting attachment of the milling machine.

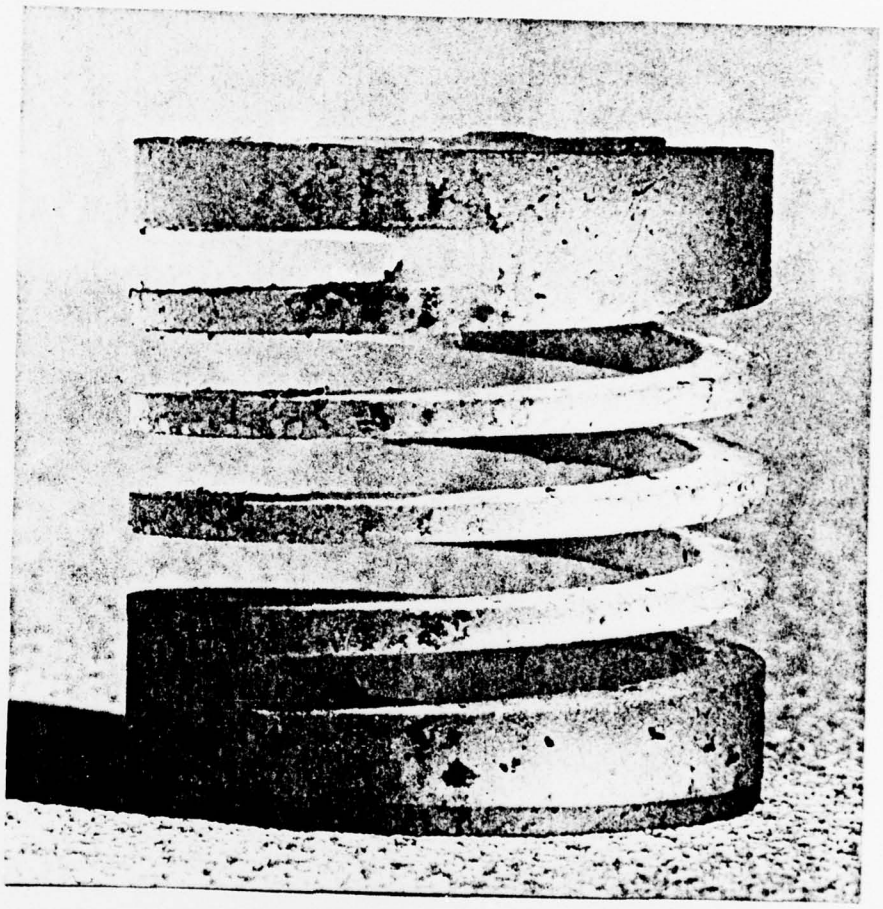

Figure 17. As fabricated helix of quartz single crystal. The overall diameter and height are both 2 cm. Specimen prepared by A. Ayensu.

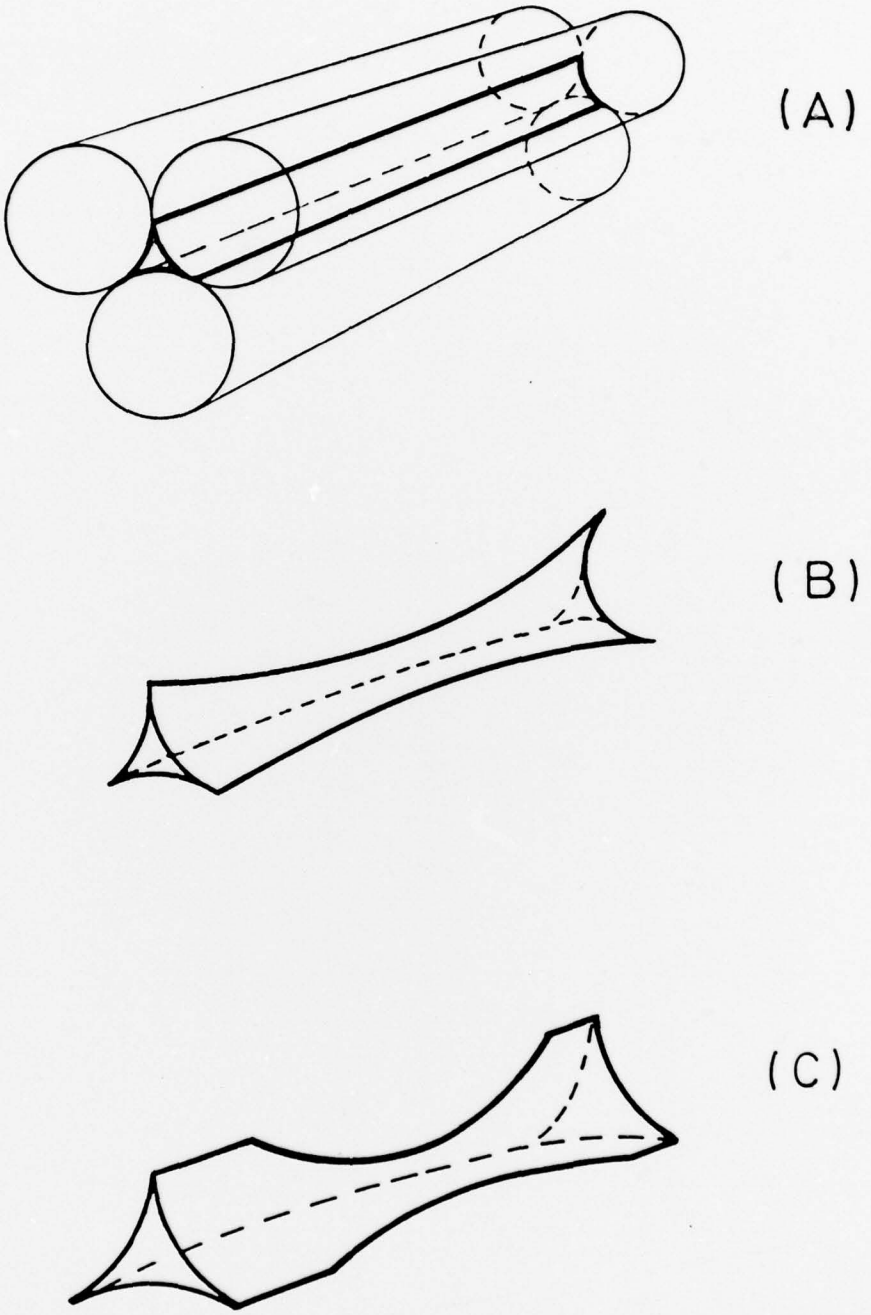

Figure 18. Shape changes in the fillet of resin between three close packed fibres.

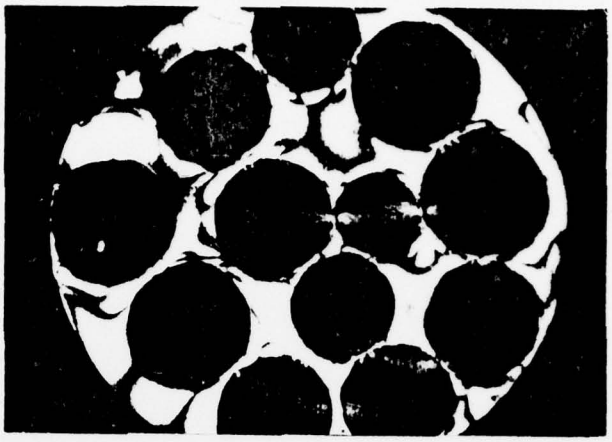

0 mm

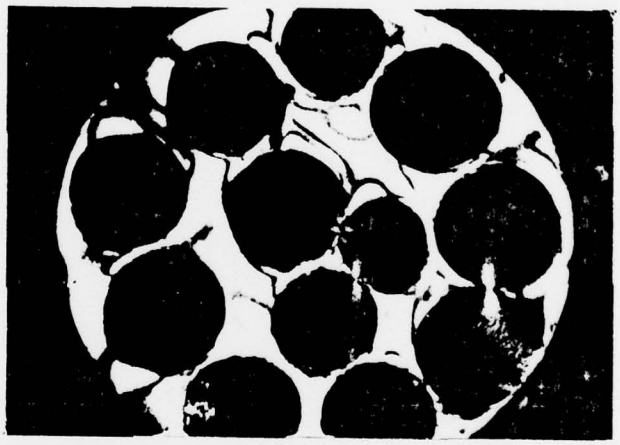

9 mm

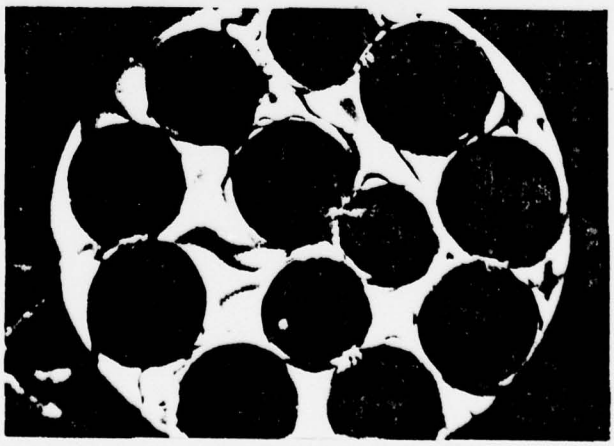

19 mm

Figure 19. Stress birefringence in the resin between fibres of 3 mm thick transverse sections through a unidirectional composite which has been exposed to hot water; the numbers denote the distance (mm) from the external surface.